

STABLE ISOTOPE COMPOSITIONS OF SURFACE WATER ACROSS  
CENTRAL MEXICO

by

JORDAN M. FOOTE

Presented to the Faculty of the Graduate School of  
The University of Texas at Arlington in Partial Fulfillment  
of the Requirements  
for the Degree of

MASTER OF SCIENCE IN EARTH AND ENVIRONMENTAL SCIENCES

THE UNIVERSITY OF TEXAS AT ARLINGTON

December 2020

Copyright © by Jordan M. Foote 2020

All Rights Reserved



## Acknowledgements

This research was supported by a grant provided by ConTex. I would like to thank Dr. Fan for her support of me and this project, as well as her mentoring under a larger project. I would also like to thank Dr. Aaron Martin, his students Carlos Daniel Torres Cardona, and Felix Gallegos Cervantes, for their help collecting river water samples in the field; Dr. Lu Zhu for helping run the HYSPLIT analysis software as well as help with R programming and data manipulation; and the staff of the Environmental Isotope Laboratory at the Iowa State University for stable isotope analysis.

November 25, 2020

## Abstract

# STABLE ISOTOPE COMPOSITIONS OF SURFACE WATER ACROSS CENTRAL MEXICO

Jordan M. Foote, MS

The University of Texas at Arlington, 2020

Supervising Professor: Majie Fan

Understanding the controlling factors of modern surface water stable isotope compositions is important for reconstructions of paleoclimate and paleoelevation. Few studies have attempted to understand patterns of surface water isotope compositions and their controlling factors in Mexico. Here I study the  $\delta^{18}\text{O}$ ,  $\delta\text{D}$  and d-excess values of 124 modern river, lake and spring water samples across the Sierra Madre Occidental, Central Mexican Plateau and Sierra Madre Oriental to constrain the spatial pattern and lapse rate. These samples were collected at various elevations after the wet season in 2019. The isotope data were integrated with moisture back trajectory analysis and climatic and geographic data to understand the controlling factors of the pattern and rate. The moistures were predominantly from oceans along

the coasts and continental recycled moisture accounts for ~17% of the total in arid Central Mexican Plateau. The isotope compositions decrease generally from coastal regions to the mountains, and the lake water isotope data display the largest variations, particularly in the arid highland in the continental interior, because of evaporation. The  $\delta^{18}\text{O}$  isotope lapse rates are small,  $-0.9\text{‰}/\text{km}$  for rivers and  $-1.4\text{‰}/\text{km}$  for springs in the Sierra Madre Occidental because of the catchment effect on both water types and evaporation of river water in the lowland. The local meteoric water lines of different water types are between 4.9 and 5.6, lower than that of the Global Meteoric Water Line, suggesting the influence of evaporation. A comparison of my surface water isotope data with previously published groundwater and precipitation isotope data suggests that the groundwater and our surface water all sourced from precipitation, and the groundwater experienced some degree of evaporation. The new understanding has implications for reconstructions of regional paleoelevation.

## Table of Contents

Acknowledgements.....	iii
Abstract.....	iv
Table of Contents.....	vi
Chapter 1 Introduction .....	1
Chapter 2 Geographic and Climatic Settings.....	5
Chapter 3 Methods.....	9
Chapter 4 Results.....	13
4.1 Climate parameters and their relationships with water isotope compositions.....	13
4.2 Vapor Trajectory.....	15
4.3 Spatial patterns of surface water isotope compositions and lapse rates.....	16
Chapter 5 Discussion.....	21
5.1 Controlling factors of isotope distribution.....	21
5.2 Isotope lapse rates.....	24
5.3 Relationship between precipitation, groundwater, river and spring water isotopic compositions.....	26
5.4 Implications for paleoaltimetry study.....	33
Chapter 6 Conclusions.....	35
Chapter 7 Future Work.....	37
Appendix A.....	39
References.....	43

## Table of Figures and Tables

Figure 1: Map of the study area.....	7
Figure 2: Elevation variations and surface water $\delta^{18}\text{O}$ values .....	8
Figure 3: 2019 Climate distribution data.....	14
Figure 4: Quantification of vapor sources.....	15
Figure 5: HYSPLIT vapor trajectories.....	17
Figure 6: Spatial distribution of isotope data.....	19
Figure 7: Local isotope data and lapse rates.....	20
Figure 8: $\delta^{18}\text{O}$ vs $\delta\text{D}$ plot showing surface water.....	27
Figure 9: Monthly average precipitation $\delta^{18}\text{O}$ values, precipitation amount and air temperature between 1962-1988 in Chihuahua.....	31
Figure 10: Monthly average precipitation $\delta^{18}\text{O}$ values, precipitation amount and air temperature between 1962-1988 in Veracruz.....	33
Table 1: Comparison of isotope values of different types of surface water in regions A and C and GNIP Veracruz station.....	30
Table 2: Table 2: Comparison of isotope values of different types of surface water in region B and GNIP Chihuahua station.....	32
Appendix A.....	39

## Chapter 1

### Introduction

Understanding of the controlling factors on modern surface water isotope compositions can be applied to the ancient surface water stable isotope compositions derived from rock records to reconstruct paleoclimate and paleoelevation (e.g., Garzzone, 2000; Bershaw et al., 2016; Zhu et al., 2018; Bershaw and Lechler, 2019). Stable hydrogen and oxygen isotope compositions of surface water record regional climatic and geographic parameters (e.g., Gat, 1996; Rowley and Garzzone, 2007; Sharp, 2007; Zhu et al., 2018). In particular, their lapse rates and seasonal changes are governed by vapor condensation temperature that is related to elevation and latitude, vapor sources (i.e. amount of recycled continental moisture), and local climate parameters of relative humidity and precipitation amount (e.g., Gupta et al., 2005; Bershaw et al., 2012; Li and Garzzone, 2017; Zhu et al., 2018; Bershaw and Lechler, 2019).

The  $\delta D$  and  $\delta^{18}O$  values of precipitation are generally controlled by temperature and vapor source isotopic composition and influenced by evaporation. The Global Meteoric Water Line (GMWL) is a regression of global meteoric water isotope compositions and has a slope of 8. The slope of any local water line can be lower than 8 due to evaporation. The smaller the slope, the greater the evaporation the water experienced. Deuterium

excess (*d-excess*), defined as  $\delta D - 8 \cdot \delta^{18}O$ , of precipitation is controlled by kinetic effects related to evaporation of the vapor source and moisture recycling at the place of condensation (e.g., Craig, 1961; Dansgaard, 1964; Poage and Chamberlain, 2001; Sharp, 2007; Hoefs, 2018). D-excess values increase in correlation with a greater moisture deficit of the ocean air masses and precipitation derived from recycled moisture, and re-evaporated moisture typically has a d-excess value greater than 10 (Gat and Airey, 2006). On a global scale, there is a strong seasonal effect on relative humidity and thus *d-excess* values, as *d-excess* is lower during summer and fall in Mexico during the rainy season because of greater precipitation and less evaporation (Sharp, 2007). Therefore, d-excess values and slope of the local precipitation can be used to understand the source of moisture and the major controlling factors of the stable isotope values.

Other forms of surface water, including groundwater, river water, spring and lake water, can be recharged by precipitation. These types of water are mostly mixtures of multiple precipitation events that typically have very large variations of isotope values, thus are good approximations of mean annual or seasonal precipitation in their catchments and can be used to study the controlling factors of the stable isotope values of precipitation as sampling mean annual or mean seasonal average precipitation is difficult

(e.g., Li and Garzzone, 2017; Zhu et al., 2018). However, complexity exists in different water types. Lowland rivers and lakes are recharged by highland precipitation as surface or subsurface runoff, as well as by direct precipitation on the lowlands. These water types can be also influenced by evaporation if the local climate is dry and the water is exposed for evaporation for long enough time (Sharp, 2007). Intense evaporation increases water  $\delta^{18}\text{O}$  and  $\delta\text{D}$  values but reduces d-excess values of residual water in arid and semi-arid regions (Gat and Airey, 2006). Variations in moisture sources within different segments of a stream should also affect its isotope pattern, if the river is long and crosses different moisture and climatic regimes. Highland water recharge reduces the lowland river  $\delta^{18}\text{O}$  and  $\delta\text{D}$  values by dilution of the heavy isotopes. Temperature difference and vapor travel distance from the water source may control the  $\delta^{18}\text{O}$  and  $\delta\text{D}$  values of precipitation, and therefore influences the overall regional pattern of river water stable isotope values (Sharp, 2007; Zhu et al., 2018).

Mexico is an arid region with multiple moisture sources and large topographic variations. There are only two stations in the Global Network of Isotopes in Precipitation (GNIP; IAEA, 2019) in Mexico, one in Veracruz and the other in Chihuahua with a distance of almost 1500 km between the two stations (Fig. 1). A previous study examined oxygen and hydrogen isotopes

in 234 shallow groundwater samples across Mexico and suggested that shallow groundwater in Mexico was mainly recharged by precipitation through infiltration, and the groundwater isotope values preferentially record summer precipitation isotope values because of abundant monsoonal precipitation (Wassenaar et al., 2009). This study also suggested that the semi-arid, central Mexican Plateau region is a low d-excess zone because of sub-cloud evaporation, and that continental recycling appears to only affect the eastern, low coastal region. However, the comparison of groundwater and precipitation isotope data in Wassenaar et al. (2009) is weakened by the insufficient spatial coverage of surface water stable isotope data. Understanding of controlling factors of surface water isotope values requires sampling different types of surface waters with good spatial coverage.

Here I study stable isotope compositions of 124 modern surface water, including river, lake and spring water along a W-E transect across different geographic domains in central Mexico in order to understand the spatial distribution of the isotope data and the controlling factors. This is the first comprehensive study of surface water stable isotope composition in Mexico.

## Chapter 2

### Geographic and Climatic Settings

Mexico's regional geography includes an internal, arid plateau region, the Mexico Plateau, bordered by two mountain regions, including the Sierra Madre Occidental mountains along the Pacific coast, and the less extensive Sierra Madre Oriental mountains near the Gulf of Mexico (Fig. 1). Across a W-E transect in the study area (Fig. 2), the elevation increases from sea level in the west coast to a mean of ~2400 m in the Sierra Madre Occidental, decreases slightly to a mean of ~2000 m in the Mexico Plateau, and rises to a mean of ~2300 m in Sierra Madre Oriental before it drops to low level in the east coast (Fig. 2) The Sierra Madre Occidental range is the largest continuous volcanic chain in the North American region (McDowell, 2007) spanning over an area of 300,000 km<sup>2</sup>. The range extends in a northwest-southeast trend, creating a drainage divide between the Pacific coastal region and the arid interior plateau. The climate adjacent to the Gulf of California and the Pacific Ocean is tropical to subtropical and adjacent to the Gulf of Mexico is tropical, whereas the interior of the continent is characterized by the Mexican Plateau desert province and is categorically arid (Morrone et al., 2002).

The Gulf of Mexico is the primary source of moisture to the east of the Sierra Madre Occidental and eastern Mexico (Fawcett et al., 2002).

Moisture to the west of the range is from the Gulf of California and greater Pacific Ocean (Stensrud et al., 1995; Schmitz and Mullen, 1996; Fawcett et al., 2002). Extreme wind convection over the western side of the range results in heavy rainfall from mid-morning until late afternoon, as far south as the lower Sinaloa region, up to northern Sonora (Barlow et al., 1998). The winds are weaker on the eastern side of the range, and therefore the low-level moisture transport is lessened. Seasonal variation of vapor source in northern Mexico is governed by the North America Monsoon (Barlow et al., 1998). The northern regions of Mexico are the most studied in terms of monsoon characteristics. The monsoon is characterized by heavy precipitation in Mexico during summer-early fall, brought by moist air from the Gulf of Mexico and the Caribbean due to the change in winds from westerly to easterly at the beginning of the monsoon (Bryson and Lowry 1955; Sellers and Hill, 1974). The monsoon mainly reaches the western slope of the high Sierra Madre Occidental and travels northward. During July–September, northwestern Mexico obtains about 70% of its total yearly rainfall from the North American Monsoon (Douglas et al., 1992). The majority of the rainfall in the southern region occurs during September and October. The source of moisture for summer precipitation is uncertain in the southwestern regions because the regions experience a

strong diurnal cycle and have rapid variations of topography that limit the accuracy of the moisture transport calculations (Barlow et al., 1997).

The rest of Mexico obtains its rainfall from the Mexican monsoon. The Mexican monsoon is an extension of the North American monsoon, where most of the annual rainfall occurs during a short period of two to four months during summer and fall. There is little agreement on the source of moisture for the Mexican monsoon as well as the thermodynamic and topographic importance in the generation of the monsoon (Barlow et al.,

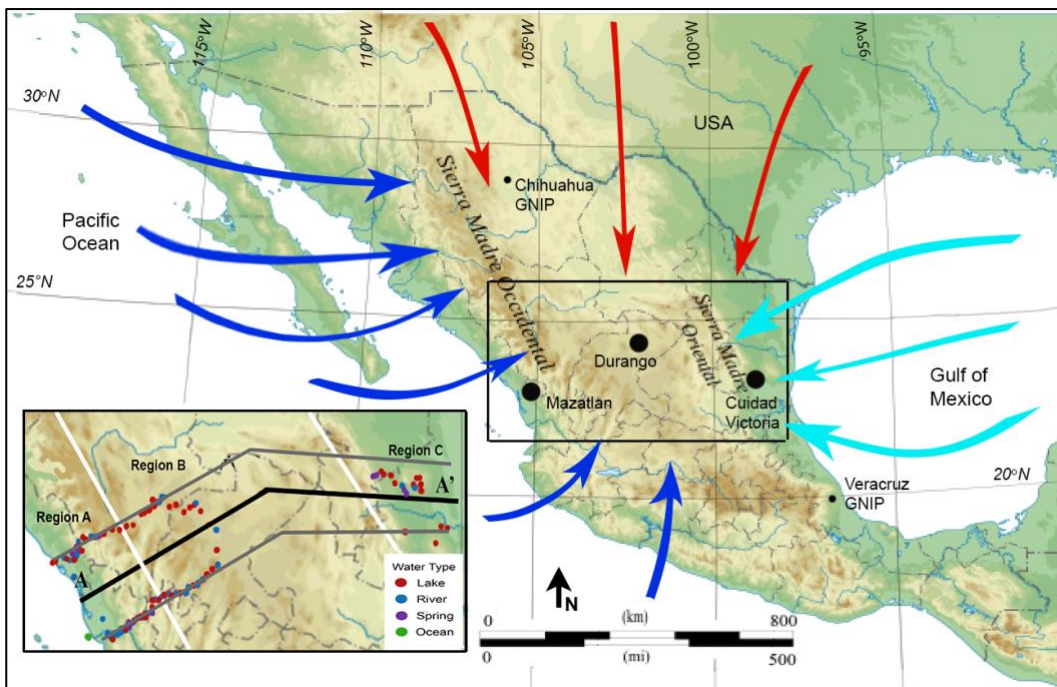


Figure 1: Map showing the study area (black box), our sampling sites (red, blue and purple dots classified by water type) and the locations of the two GNIP stations in Mexico. Each color arrow represents a different vapor source (Dark blue is for Pacific Ocean, red is for continent US and light blue is for Gulf of Mexico). Elevation variations across central Mexico along the three lines are shown in Figure 2.

1997). This monsoon's influential factors appear to be correlative to those that affect the major North American monsoon, including deep heating in the monsoonal air trajectory pattern, the elevated heating of the proximal mountains and plateau, and orographic forcing due to seasonal shift (Barlow et al., 1997).

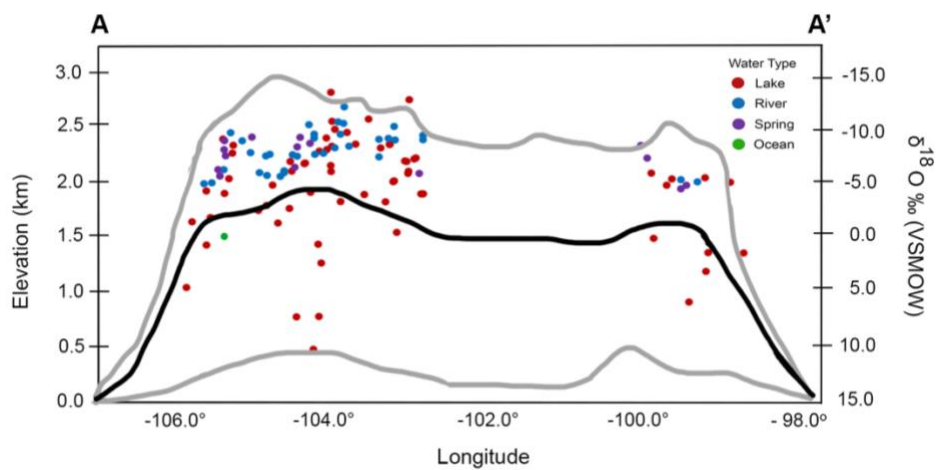


Figure 2: Elevation variations and surface water  $\delta^{18}\text{O}$  values within the study region, from west coast to east coast. The two gray and one black line show the elevation variations along the three lines in Figure 1.

## Chapter 3

### Methodology

A total of 124 water samples were collected in October and November 2019, right after the monsoon season. Locations, elevations, sampling date and water types are listed in Appendix A. Samples were collected along two transects crossing the Sierra Madre Occidental range (Fig. 1). Samples along the northern transect were obtained near or along Interstate 40 between Durango and Mazatlán and along HWY 15D between Mazatlán and Santiago Ixcuintla. The southern transect was sampled along HWY 44 between the west coast and Fresnillo and along HWY 49 between Fresnillo and Juan Aldama. Samples were also collected between Durango and Ciudad Victoria, crossing the Sierra Madre Oriental mountains. These east-west trending highways cross the mountain ranges, allowing access at multiple altitudes. We sampled both large and small surficial flowing streams, spring water flowing out from underground or seeping out of rocks, as well as ponds and lakes of various sizes (lumped as lake samples). We also sampled one ocean surface water sample. The water samples were obtained and stored in 15 ml plastic vials, sealed by a screw top and Teflon tape, to ensure a proper seal, and placed in a chilled cooler to limit, if not avoid, evaporation.

Climatic parameters, including mean annual temperature, total yearly precipitation, and mean annual relative humidity (RH) in Mexico, were extracted from the average yearly data of global climate data (NOAA, 2019).

Moisture trajectories in each river drainage during the spring and summer seasons were modeled using the Hybrid Single-Particle Lagrangian Integrated Trajectory model (HYSPLIT, Draxler and Rolph, 2014) in order to track the sources of precipitation before and during the sampling seasons. We conducted moisture trajectory analyses for the cities of Ciudad Victoria (east), Durango (central), and Mazatlán (west). For reference analysis, we also conducted moisture trajectory for the two GNIP sites. For each representative locality, back trajectories were computed every 6 hours during October-November for the fall of 2019. We use 120-hour total backwards trajectories for each individual vapor trajectory analysis. Moisture sources were determined based on the locations of the end points of vapor back trajectories. While it is not guaranteed that the ultimate source can be determined by the analysis, the relative contribution of each source of the precipitation can be well approximated based on the end points of the back trajectories. The initial air parcel was set at 1 km above ground, because most atmospheric moisture is in the lower troposphere (0–2 km above ground level) and there is no significant

difference in results for initiation at 0.5, 1.0, or 1.5 km level (Li and Garziona, 2017). Among the computed results of back trajectories, we only considered the trajectories that produced rain at the study area during the sampling periods. Filtering of data was determined by data cleansing in R-Studio. At each representative locality, the contribution of each rain-producing trajectory was determined based on its precipitation volume. The contribution of each source was determined by the sum of its contribution to all precipitation episodes in the season and the number of backwards trajectory endpoints within a major moisture origin. My sampling locations were loaded into ArcGIS along with a raster digital elevation map and transformed by use of spatial analysis extension tools to demonstrate hydrology parameters. These data were extrapolated to quantify the hypsometric drainage elevation for each of the sampling sites.

Samples were measured via a Picarro L2130-i Isotopic Liquid Water Analyzer, with autosampler and ChemCorrect software in the Isotope Laboratory at the Iowa State University. Each sample was measured a total of six times. To account for memory effects, only the last three injections were used to calculate mean isotopic values. Reference standards (USGS 47, USGS 48) were used for regression-based isotopic corrections. At least one lab standard was analyzed after every five samples to monitor system drift. The uncertainty, including analytical uncertainty determined from

multiple injections and average correction factor, is less than 0.07‰ for  $\delta^{18}\text{O}$  and 0.34‰ for  $\delta\text{D}$  (VSMOW) for all the samples.

## Chapter 4

### Results

#### 4.1 Climate parameters and their relationships with water isotope compositions

In central Mexico, the annual precipitation varies between 4 mm and 38 mm and the majority area receives more than 10.5 mm precipitation (Fig. 3A). The mountains generally have higher precipitation than the central plateau and the greatest precipitation occurs in the coastal regions. The average relative humidity (RH) varies between 26% and 100% and the majority of the study area has an RH higher than 43% (Fig. 3B). The mountains generally have higher RH than the central plateau, and the highest RH is in the coastal regions. The average annual temperature varies between 10 °C and 17 °C (Fig. 3C). The temperature is comparable in the mountains and central plateau and is high in the coastal regions.

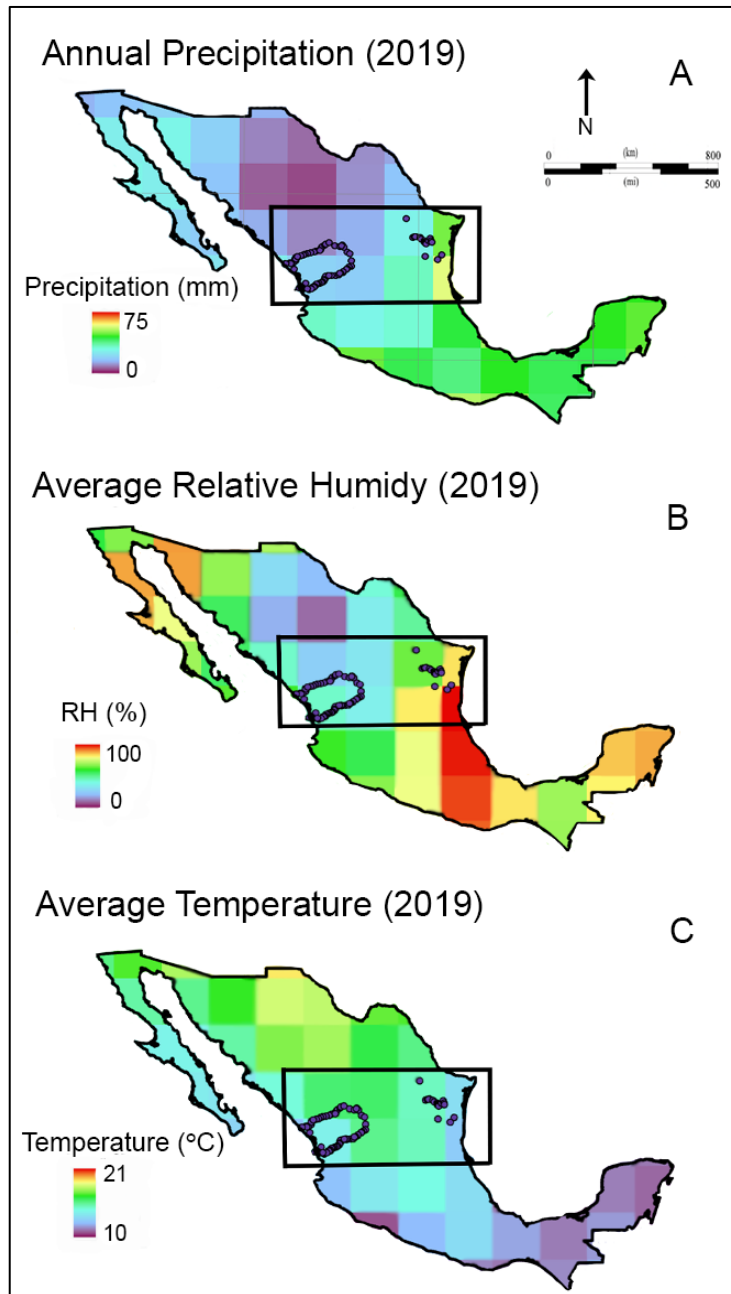


Figure 3: Climate parameters for Mexico in 2019. A) Annual precipitation volume, B) Average relative humidity, C) Average temperature. Derived from global climate data for 2019.

## 4.2 Vapor Trajectory

The contribution of each moisture source to local precipitation varies spatially during the sampling season (Fig. 4). In Mazatlán, on the west coast, moistures were predominantly from the Pacific Ocean (96%), with a minor amount from continental recycling (4%). In Durango in central Mexico,

moistures were from the Pacific (34%), Gulf of Mexico (49%) and continental recycling (17%). In Cuidad Victoria (CV), near the east coast, moistures were mainly from the Gulf of Mexico (82%), with minor contribution from the Pacific (7%) and continental

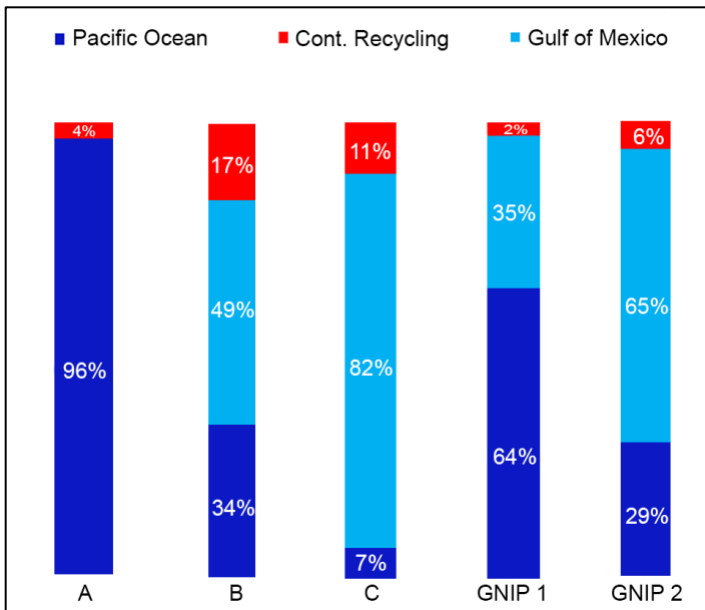


Figure 4: Quantification of vapor sources of the three representative cities in the study area and the two GNIP stations in September and October, 2019. A: Mazatlán in west coast, B: Durango in central Mexico, C: Cuidad Victoria in east coast, GNIP 1: Station in Chihuahua, GNIP 2: Station in Veracruz. (<https://nucleus.iaea.org/wiser>).

recycling (11%). For comparison, moistures in Chihuahua, in northern Mexico were from the Pacific (65%), Gulf of Mexico (35%), and continental recycling (2%); and moistures in Veracruz, in southern Mexico, were from

the Gulf of Mexico (65%), Pacific (29%), and continental recycling (6%). In summary, in the study area, moistures are mainly from the Pacific for western coast and the Gulf of Mexico for eastern coast, and the contributions from the two sources are nearly equal in central Mexico.

#### 4.3 Spatial patterns of surface water isotope compositions and lapse rates

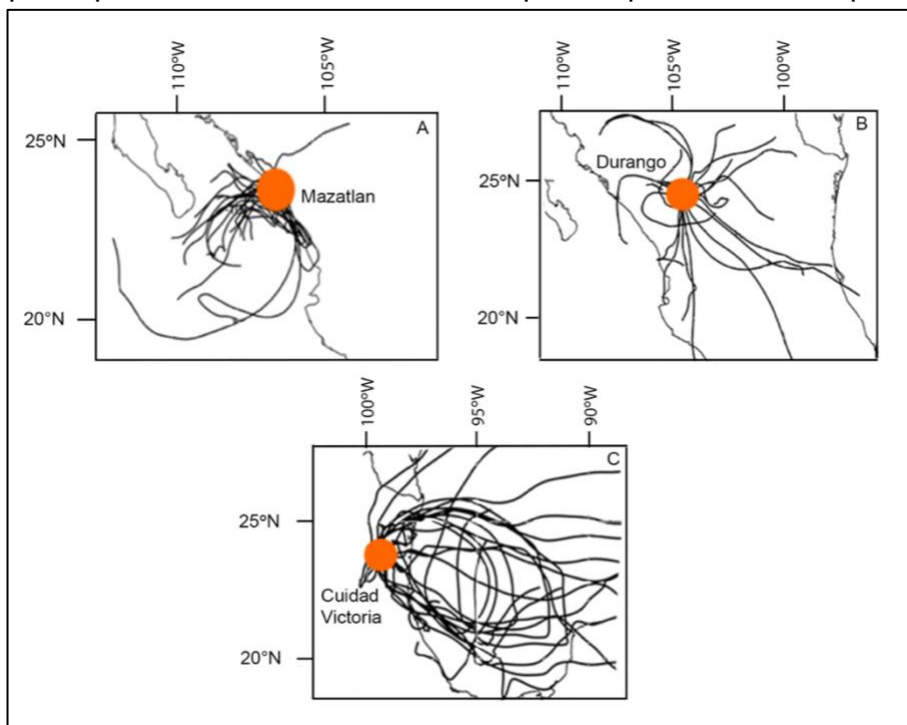


Figure 5: HYSPLIT vapor trajectories for precipitation during September and October 2019 at three representative sites in Regions A, B and C.

The  $\delta^{18}\text{O}$ ,  $\delta\text{D}$ , and d-excess values of the river water samples vary from -11.9 to -5.4‰, -88.2 to -29.5‰, and -5.8 to 16.5‰, respectively (Fig. 6; Appendix A). I divided the study area into three regions (A-C, Fig.1)

based on topography and moisture sources. Region A is located to the west from the Pacific coast to the Sierra Madre Occidental peaks. The region obtains moisture from the Pacific Ocean predominantly. The central plateau encompasses region B from the eastern slopes of the Sierra Madre Occidental to the eastern Sierra Madre Oriental. The region receives a mixture vapor sources. Region C is between the Sierra Madre Oriental peaks and coast of the Gulf of Mexico where it receives the majority of its moisture. The  $\delta^{18}\text{O}$  and  $\delta\text{D}$  values decrease while the d-excess increases from the coastal regions toward mountains in regions A and C. The southern end of the Sierra Madre Occidental in region B has the lowest  $\delta^{18}\text{O}$  and  $\delta\text{D}$  values, but the northern end has the highest  $\delta^{18}\text{O}$  and lowest d-excess values (Fig. 6). Because the distribution patterns of  $\delta^{18}\text{O}$  and  $\delta\text{D}$  values are similar, I only describe and discuss the  $\delta^{18}\text{O}$  and the d-excess values.

The lake water samples have a wide range of isotope values and the lowest slope of local meteoric water line (LMWL) slope the three water types. The spring and river water LMWLs closely resemble GMWL and have smaller isotope ranges. The lapse rate of all water types across the study area is  $-1.29\text{‰}/\text{km}$  (Fig. 7) but varies in different regions.

In region A, to the west of the peak of Sierra Madre Occidental, the  $\delta^{18}\text{O}$  values range from  $-70$  to  $-10\text{‰}$ . The d-excess values ( $-19.3$  to  $16.5\text{‰}$ )

are between the values of region B and C. Linear regressions of the isotope values generate LMWLs of  $y = 7.1x + 5.9$  ( $R^2 = 0.89$ ;  $n=20$ ) for river water,  $y = 5.6x - 9.02$  ( $R^2 = 0.94$ ;  $n=20$ ) for lake water, and  $y = 7.9x + 12.8$  ( $R^2 = 0.98$ ;  $n=10$ ) for spring water (Fig. 7). The  $\delta^{18}\text{O}$  values of river and spring water are inversely correlated to mean drainage elevations, and the local lapse rate is  $-1.4\text{‰}/\text{km}$  for spring water, and  $-0.9\text{‰}/\text{km}$  for river water across 2.8 km elevation change (Fig. 7).

In region B in central Mexico, the  $\delta^{18}\text{O}$  values range from  $-80$  to  $-15\text{‰}$ , generally lower than those in region A. The d-excess values are the lowest in my study area ( $-59.2$  to  $14.7\text{‰}$ ). Linear regressions of the isotope values generate LMWLs of  $y = 5.7x - 15.3$  ( $R^2 = 0.76$ ;  $n= 18$ ) for river water, and  $y = 5.2x - 21.6$  ( $R^2 = 0.97$ ;  $n= 29$ ) for lake water (Fig. 7). There are no statistically significant correlations between  $\delta^{18}\text{O}$  values of river and lake water and mean drainage elevations.

In region C to the east of the peak of Sierra Madre Oriental, the  $\delta^{18}\text{O}$  values range from  $-35$  to  $15\text{‰}$ , and the d-excess values are relatively high ( $-22.0$  to  $17.0\text{‰}$ ) across 0.69 km elevation change. Fewer samples of river water were collected in region C than in the other two regions, thus a LWML cannot be generated for river water. The LWMLs are  $y = 4.9x - 6.1$  ( $R^2 = 0.96$ ;  $n=11$ ) for lake water, and  $y = 5.8x - 2.2$  ( $R^2 = 0.99$ ;  $n=4$ ) for spring water

(Fig. 7). The  $\delta^{18}\text{O}$  values of the spring water are inversely correlated to mean drainage elevations with a high local lapse rate of  $-8.6\text{‰}/\text{km}$  (Fig. 7).

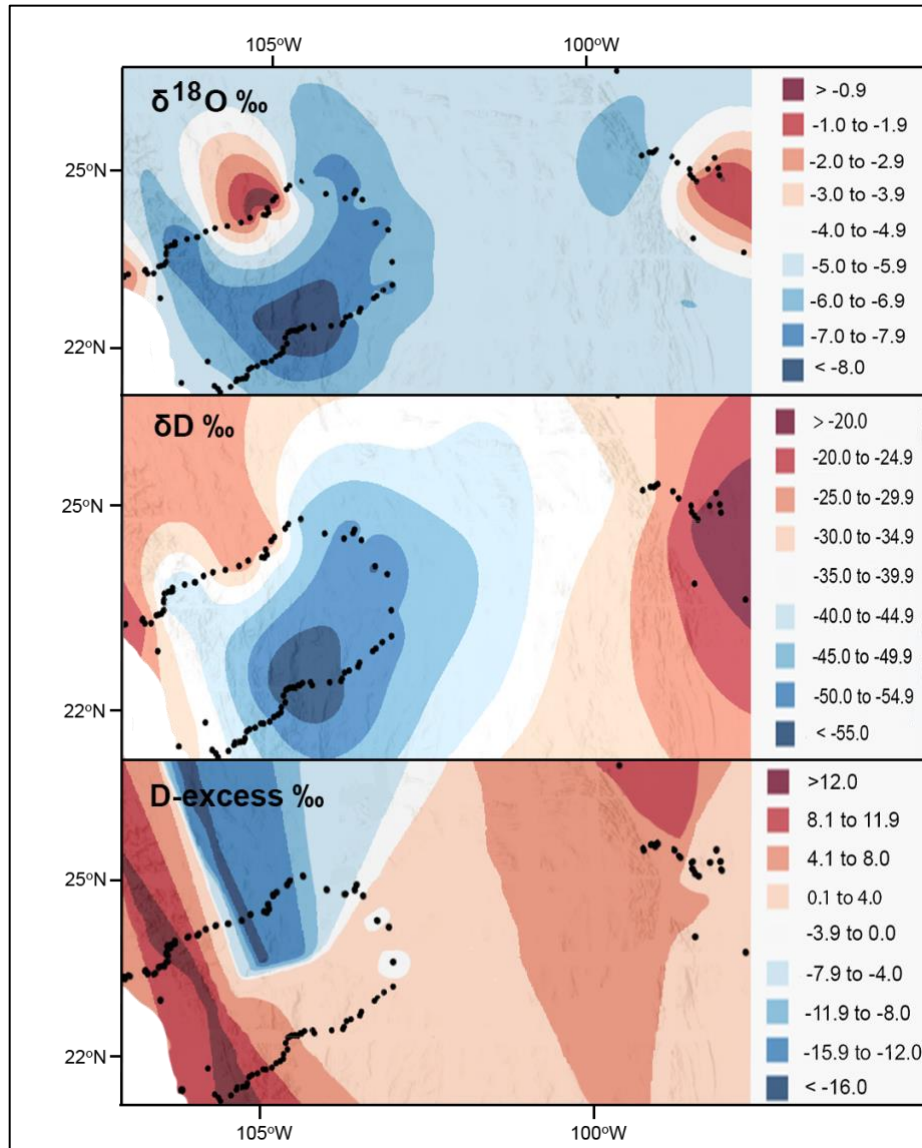


Figure 6: Spatial distributions of d-excess,  $\delta\text{D}$  and  $\delta^{18}\text{O}$  values of surface water in the study area.

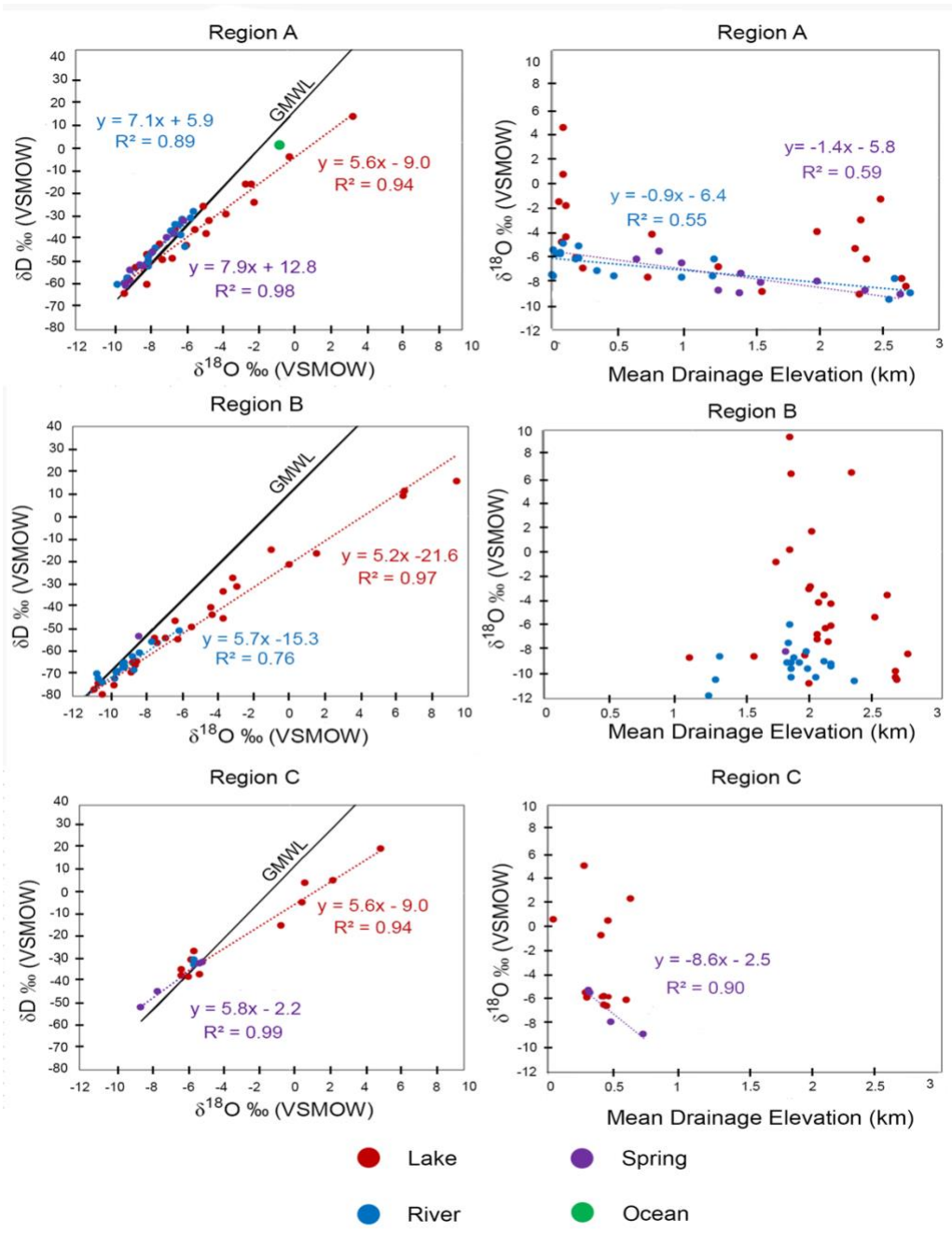


Figure 7: Plots showing  $\delta^{18}O$  vs.  $\delta D$  values and  $\delta^{18}O$  vs. mean drainage elevations of the three water types. Region A is the Sierra Madre Occidental region, Region B is the Central Mexican Plateau, and region C is the Sierra Madre Oriental.

## Chapter 5

### Discussion

#### 5.1 Controlling factors of isotope distribution

Air temperature is the most important environmental factor of precipitation stable isotope values because it controls the isotope fractionation of vapor condensation. Other factors include latitude, altitude, continentality, precipitation amount and seasonality that partially influence isotope values because of temperature change (e.g., Dansgaard, 1964; Bagheri, 2019). Precipitation isotope values are also influenced by sub-cloud evaporation because of low relative humidity (e.g., Gat, 1996; Yurtsever 1975; Hoefs, 2018). In addition to precipitation, surface water including river water, groundwater and spring water have complicated water origins and the isotope values are often influenced by post-precipitation evaporation and catchment effect (e.g., Craig, 1961; Wassenaar, 2009; Bershaw et al., 2012; Zhu et al., 2018). It is generally thought that river water integrates precipitation in the upper catchment and its isotope values reflect the precipitation isotope values at the hypsometric elevation of the river catchment, which are typically lower than those of local precipitation (e.g., Dutton et al., 2005; Rowley and Garzzone, 2007; Li and Garizone, 2017; Zhu et al., 2018).

My integration of surface water stable isotope data, climate data, and vapor trajectory analysis show that temperature, elevation, vapor sources and evaporation are the key controls on the surface water isotope distribution patterns in central Mexico. The most straightforward observation of the dataset is that the surface water isotope values decrease as elevation increases from both the west and east coasts towards the Sierra Madre Occidental and Oriental mountains (Figs. 2 and 5). This pattern reflects gradual depletion of heavy isotopes associated with progressive rainout as the vapors derived from the oceans ascend topography and experience adiabatic expansion and cooling (Dansgaard, 1953, 1964; 1980; Gat, 2000; Poage and Chamberlain, 2001; Rowley and Garzione, 2007).

D-excess values and slopes of the local precipitation can be used to aid in understanding of the controls of surface water isotope values (Gat, 1981; Kumar et al., 2018). While kinetic evaporation processes in moisture sources and in sub-cloud layers both increase precipitation d-excess, post-precipitation surface evaporation decreases surface water d-excess (Gat and Airey, 2006). Precipitation derived from recycled moisture typically has a d-excess greater than that (10‰) of the GMWL. In the study area, coastal regions have higher d-excess values than the continental interior (Fig. 6), consistent with the observation made from ground water in Mexico

(Wassenaar et al., 2009), suggesting that surface water in the continental interior experienced post-precipitation evaporation. Regions A and C have similar ranges of elevation (Fig. 2) but different primary moisture sources, and the  $\delta$ -excesses of Region C are lower compared to those in Region A (Fig. 7), suggesting that the two different vapor sources experienced different degrees of evaporation at the ocean surface. Region B has low  $\delta$ -excess values (Fig. 6), arid climate (Fig. 3) and abundant recycled moisture (Fig. 4), supporting the interpretation that evaporation influences surface water isotope values in continental interior.

Slopes of LMWLs can be also used to assess the influence of evaporation. Waters that experienced evaporation have a slope less than 8 (Craig 1961; Gat 1996). The data show differences in LMWL slopes (Fig. 6), reflecting variation in the degree of evaporation. The slopes (7.1, 5.6) of the river and lake water lines in region A are higher than those (5.7, 5.2) in region B (Fig. 7), consistent with the interpretation of greater evaporation in arid region B based on  $\delta$ -excess values. In region B, lake water isotope values also show the largest variation (Fig. 6), supporting the interpretation that intense evaporation occurs in the region, particularly in the northern end of the Sierra Madre Occidental and in the central plateau region. Interestingly, region C has the highest RH and precipitation, but the lowest slopes (5.8, 4.9) for the river and lake water lines among the three regions,

likely a result of evaporation because the samples were taken longer after the major rain compared to the other regions (Appendix A).

## 5.2 Isotope lapse rates

The progressive depletion of  $^{18}\text{O}$  and D in orographic precipitation leads to an isotopic lapse rate (e.g., Poage and Chamberlain, 2001), which has been commonly used to reconstruct paleoelevation of mountains and plateaus (e.g., Garzione et al., 2000; Zhu et al., 2018). Surface water isotope lapse rates are mostly controlled by temperature dependent isotope fractionation, but are also influenced by other factors such as catchment effect and post-precipitation evaporation in regions with low RH (e.g., Dutton et al., 2005; Rowley and Garzione, 2007; Zhu et al., 2018). Because the lake water isotope values are heavily influenced by evaporation, I only discuss river and spring water isotope lapse rates.

In Region A, the oxygen isotope lapse rates of spring water (-1.4 ‰/km) and river water (-0.9 ‰/km; Fig. 7) are both smaller than the average global precipitation lapse rate (-2.8 ‰/km; Poage and Chamberlain, 2001). Possible explanations for the low lapse rate include evaporation, addition of recycled moisture to precipitation that contributed to the highland surface water, and catchment effect on the lowland surface water. Evaporation increases surface water  $\delta^{18}\text{O}$  and  $\delta\text{D}$  values and reduces d-excess below

the global average (Gat and Airey, 2006). At the highlands of the Sierra Madre Occidental in region A, the river and spring water isotope values are the lowest, while the d-excess values are slightly higher than global average (Fig. 6). These observations are the opposite of the effects of evaporation, suggesting that the highland water in the Sierra Madre Occidental in region A did not experience evaporation. The high d-excess at the highlands is a result of recycled moisture, which only contributes 4-17% of the precipitation in central Mexico (Fig. 4). Given that the isotope values of the recycled moisture are not known, and its contribution is low, its influence on the low isotope lapse rate should be small. It has been documented in several studies that catchment effect (highland river water charges lowland river) makes river water isotope values lower than those of local precipitation (e.g., Dutton et al., 2005; Rowley and Garzzone, 2007; Zhu et al., 2018). Therefore, catchment effect is the major cause of the low lapse rate of river water in region A. The low lapse rate of spring water is also a result of catchment effect of shallow groundwater, which is the major source of spring water. The lapse rate of the spring water is higher than that of the river water, suggesting local precipitation contributed more water to lowland groundwater than river water.

The rivers in Region B do not have a lapse rate (Fig. 7) because of small variation in elevation in the sampling region. In Region C, the spring

water has an oxygen isotope lapse rate of  $-8.6\text{‰}/\text{km}$ , much steeper than the global average (Fig. 7). However, this rate is derived from only four samples with an elevation range of 0.5 km, thus has low statistical significance. If the rate is of significance, it is most likely a result of evaporation of lowland water. This interpretation is supported by that the local spring and lake water lines both have small slopes ( $< 6$ ), and the  $d$ -excess values are smallest adjacent to the coast (Fig. 6).

### 5.3 Relationship between precipitation, groundwater, river and spring water isotopic compositions

I compared my surface water isotope data with those of the published monthly precipitation from the two GNIP stations (IAEA, 2019) and the groundwater in Mexico (Wassenaar et al., 2009) in order to understand the relationship between the waters (Fig. 8). The surface water isotope data from central Mexico are mostly clustered around the GMWL, with some of my river and lake water samples below the GMWL as a result of evaporation.

The surface water isotope data in Region A and C were compared to the groundwater in the same regions, and the precipitation in Veracruz because they all receive moisture predominantly from the adjacent oceans (Table 1). The GNIP precipitation isotope data are averages of

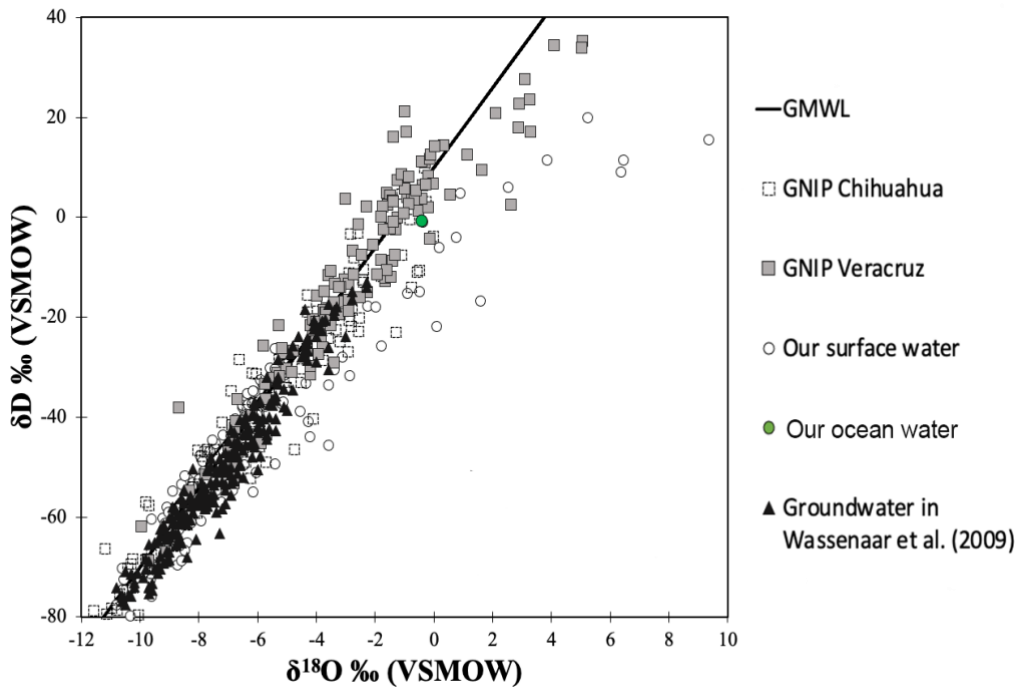


Figure 8: Plot of  $\delta^{18}\text{O}$  vs.  $\delta\text{D}$  of different types of surface water in central Mexico.

precipitations in each month for years 1962-1988. A total of 136 data were used to calculate monthly averages to examine the controls of temperature and precipitation amount on precipitation isotope values (Fig. 9). The monthly average  $\delta^{18}\text{O}$  values are between  $-5.2\text{‰}$  and  $0.5\text{‰}$  with high values in winter and low values in summer, and the d-excess values are between  $2.3\text{‰}$  and  $9.0\text{‰}$  with low values in spring and high values in late fall.

The monthly average  $\delta^{18}\text{O}$  values are negatively correlated to both air temperatures and monthly average precipitation amounts (Fig. 9).

Because precipitation  $\delta^{18}\text{O}$  values increase as condensation temperature increases, the correlations suggest that precipitation amount is a major control of the isotope values. This is typical of a monsoonal climate. The comparisons of different water types in Table 1 show that 1) the ranges of lake water  $\delta^{18}\text{O}$  values in Regions A and C are greater than those of monthly precipitation in Veracruz and groundwater because lake water is influenced by intense evaporation. The range of lake water in region A is the greatest among all water types because of altitude effect on the lowest isotope values and evaporation effect on the highest values; 2) the range of groundwater  $\delta^{18}\text{O}$  values is similar to those of spring water, river water, and monthly average of precipitation, suggesting that the spring, river and ground water all were charged by precipitation; and 3) many of the groundwater d-excess values are less than 10‰, comparable to those of the river water, suggesting that the groundwater in Regions A and C only experienced some degree of evaporation, this is different from the assumption in Wassenaar et al. (2009) that groundwater in Mexico did not experience evaporation. The evaporation most likely happens in vadose zones, before the deep infiltration of precipitation water (Zhu et al., 2018).

Table 1: Comparison of isotope values of different types of surface water in regions A and C and GNIP Veracruz station.

Water Type	$\delta^{18}\text{O}$	$\delta\text{D}$	d-excess	Notes
Region A Lake (n=20)	-9.3 to 3.8‰	-64.8 to 11.4‰	-19.3 to 16.1‰	Evidence of strong evaporation (positive values and low d-excess)
Region A River (n=18)	-9.6 to - 5.2‰	-60.5 to - 29.5‰	2.0 to 16.5‰	Evidence of evaporation (low d-excess)
Region A Groundwater (n=17)	-10.1 to - 4.8‰	-71.3 to - 34.4‰	3.5 to 10.1‰	Evidence of evaporation (low d-excess)
Region C Lake (n=11)	-6.2 to 5.2‰	-37.9 to 19.9‰	-22.0 to 17.0‰	Evidence of strong evaporation (positive values and low d-excess)
Region C River (n=2)	-5.4‰	-32.5 to - 30.4‰	11.0 to 12.9‰	No evaporation
Region C Spring (n=4)	-8.5 to - 4.9‰	-51.8 to - 31.0‰	8.7 to 16.0‰	No evaporation
Region C Groundwater (n=21)	-8.9 to - 3.0‰	-60.2 to - 17.5‰	-0.4 to 13.2‰	Evidence of evaporation (low d-excess)
Precipitation Veracruz (n=136)	-12.0 to 5.0‰	-89.0 to 35.0‰	-18.5 to 31.3‰	Large variations of rain events

The isotope data in Region B were compared to those of groundwater in the same region and the precipitation data in Chihuahua because the regions are both semi-arid and receive a great portion of

recycled moisture (Table 2). A total of 125 isotope data from the GNIP Chihuahua station were used to calculate monthly averages to examine the controls of temperature and precipitation amount (Fig. 10). The monthly average  $\delta^{18}\text{O}$  values are between  $-11.7\text{‰}$  and  $-5.3\text{‰}$  with high values in summer and low values in winter. The monthly average d-excess values are between  $0.9\text{‰}$  and  $7.7\text{‰}$  with high values in summer and low values in winter. The high d-excess values suggest contribution of recycled moisture in precipitation. The monthly average  $\delta^{18}\text{O}$  values are correlated to air temperatures but not monthly average precipitation amounts, suggesting that temperature is the major control of the precipitation isotope values. The comparisons also show that 1) the range of lake water  $\delta^{18}\text{O}$  values is greater than those of monthly precipitation and groundwater because lake water is influenced by intense evaporation; 2) the range of groundwater  $\delta^{18}\text{O}$  values is similar to those of spring water, river water, and monthly average of precipitation, suggesting the spring, river and ground water were all charged by precipitation; and 3) most of the groundwater d-excess values are less than  $10\text{‰}$ , lower than those of the river water, suggesting that the groundwater in Region B experienced more evaporation than the river water. The degree of evaporation of groundwater in Region B is more intense compared to that in Regions A and C because of semi-arid regional climate.

Table 2: Comparison of isotope values of different types of surface water in region B and GNIP Chihuahua station

Water Type	$\delta^{18}\text{O}$	$\delta\text{D}$	d-excess	Notes
Region B Lake (n=29)	-13.2 to 9.3‰	-97.2 to 15.5‰	-59.2 to 10.8‰	Evidence of evaporation (positive values and low d-excess)
Region B River (n=18)	-11.9 to -6.1‰	-88.2 to -51.0‰	-5.8 to 14.7‰	Evidence of evaporation (low d-excess)
Region B Spring (n=1)	-8.3‰	-54.0‰	12.0‰	No evaporation
Groundwater Region B (n=53)	-10.4 to -5.1‰	-75.8 to -37.4‰	-4.8 to 13.1‰	Evidence of evaporation (low d-excess)
Precipitation Chihuahua (n=125)	-14.0 to 0.0‰	-97.0 to 10.0‰	-12.7 to 27.0‰	Large variations of rain events

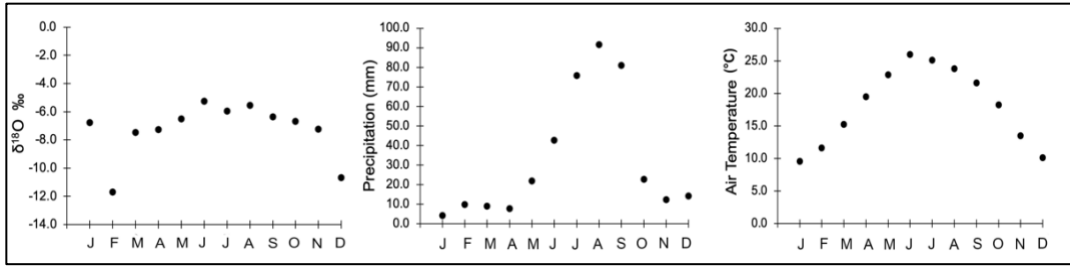


Figure 9: Monthly average precipitation  $\delta^{18}\text{O}$  values, precipitation amount and air temperature between 1962-1988 in Chihuahua at 1.42 km.

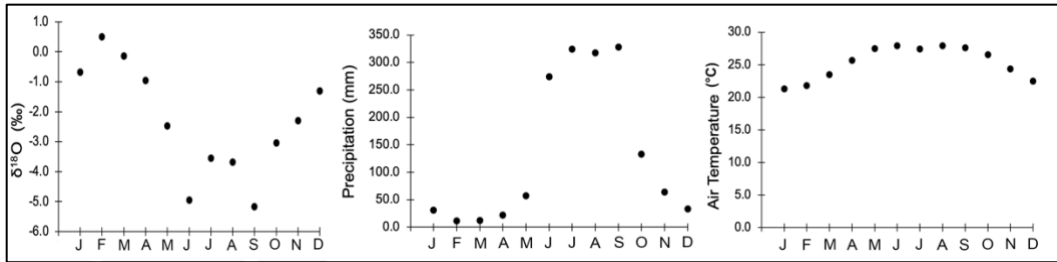


Figure 10: Monthly average precipitation  $\delta^{18}\text{O}$  values, precipitation amount and air temperature between 1962-1988 in Veracruz at 0.02 km.

In summary, the comparison of isotope values of different types of surface water in Mexico suggests that groundwater, lake, spring and river water all are from local precipitation. The groundwater experienced some degree of evaporation, not as intense as the lake water, but nearly comparable to that of the river water in the semi-arid continental interior.

#### 5.4 Implications for paleoaltimetry study

The topographic history of the Sierra Madre mountains is not well understood. The understanding of modern surface water isotope values in the region sets the foundation for stable isotope paleoelevation reconstruction of the mountains. Many studies have applied modern isotope lapse rates to reconstruct paleoelevation of mountain belts, offering important insights on the tectonic processes of orogenesis (e.g., Fan et al., 2014; Bershaw et al., 2016; Jackson et al., 2019).

Stable isotope paleoaltimetry uses surface water isotope compositions preserved in minerals as well as isotope lapse rates to determine elevation at the time of mineral formation. Such surface water isotope values can be surface water  $\delta^{18}\text{O}$  values reconstructed from various carbonate minerals and surface water  $\delta\text{D}$  values reconstructed from hydrated volcanic glass (e.g., Fan et al., 2014; Bershaw et al., 2016; Jackson et al., 2019; Zhu et al., 2018). There are Cenozoic volcanic fields within the Sierra Madre Occidental range that have produced volcanic glass in tuffs (McDowell, 2007) and the  $\delta\text{D}$  values of the fully hydrated volcanic glass can be used for paleoelevation study of the mountains.

This study is the first to present a regional stable isotope lapse rate and its controlling factors in the Mexico. The modern water isotope values show spatial variations and the regional isotope lapse rate is influenced by

evaporation and catchment effect. Although seasonal variations of the lapse rate are not examined, I predict that the rate changes as a result of changing degree of evaporation and precipitation amount, similarly as in the central Rocky Mountains in the USA (Zhu et al., 2018). The understanding brings caution to apply the lapse rate for paleoelevation reconstruction as paleoclimate must be carefully evaluated. The data show that lake water can be intensively evaporated, and river and groundwater also experience some degree of evaporation, particularly in the semi-arid Central Plateau region. If surface water  $\delta^{18}\text{O}$  values are reconstructed from lacustrine carbonate and shallow groundwater carbonate cement for paleoelevation reconstructions, the degree of evaporation must be considered. Similarly, volcanic glass may be deposited in lake and river water that has experienced evaporation. Therefore, depositional environment of the carbonate minerals and volcanic glass must be well studied for correct interpretation of stable isotope data and paleoelevation reconstruction.

## Chapter 6

### Conclusions

This project studies the variation of surface water stable isotope compositions along an E-W transect across the Sierra Madre Occidental, Central Mexican Plateau and the Sierra Madre Oriental mountains in Mexico. The project integrates back trajectory analysis of precipitation and climate and geographic parameters to examine the controlling factors of the spatial patterns of surface water isotope values. The vapor trajectory analysis shows that the Sierra Madre Oriental and Occidental receive moisture predominantly from the Gulf of Mexico, and Pacific Ocean, respectively, while the Central Plateau in continental interior receives a mix of both and ~17% of recycled continental moisture.

A comparison of isotope data of my river, lake, and spring water with those of published groundwater and GNIP precipitation suggest that the surface water was derived from local precipitation and experienced various degrees of evaporation. The results show that the lake water experienced intense evaporation, and the local oxygen isotope lapse rate of river water is ~0.9‰/km in the Sierra Marda Occidental, much lower than global average, which we attribute to catchment effect, as highland precipitation with low  $\delta^{18}\text{O}$  values contributes to lowland river discharge, and some degree of evaporation in the lowlands. The evaporation of river water and

groundwater most likely occurs to local precipitation in the vadose zones of river catchments before deep filtration.

The local lapse rate and understanding of the controlling factors on surface water isotope compositions have implications for paleoelevation reconstruction. I suggest that paleoclimate and depositional environments of carbonate and volcanic glass samples must be evaluated in order to constrain the influence of evaporation and vapor mixing on water isotope data of different surface water types.

## Chapter 7

### Future Work

Future work to continue the investigation of this project includes resampling water at the same locations in the spring in order to characterize the isotope distribution in dry season. A comparison of the isotope data in the dry season with the data of the wet season presented in this study can bring understanding of the controlling factors on temporal differences. Sampling in this project took place one week after the rainy season and much of the surface water may have been evaporated so an additional sampling during the wet, rainy season may also be useful. In addition, an understanding of water transport would be useful as water use by humans may have affected the availability of surface water to sample. Due to the arid climate, water resources are lacking, and movement of water becomes necessary. Irrigation and pumping and water transport trucks that bring water to villages and towns for human consumption and farming could lead to decrease of river and groundwater flow rates, promoting the influence of evaporation on isotope values. River water isotope values are often used as a good approximation of event-averaged precipitation isotope in a broad catchment region (Kendall and Coplen, 2001; Dutton et al., 2005), sampling surface water immediately after or during the rainy season would limit the

influence of evaporation, and such data may be a better approximation of the average precipitation.

## Appendix A. Surface water data presented in this study

ID	Sample Type	$\delta^{18}\text{O}$ (VSMOW)	$\delta\text{D}$ (VSMOW)	d-excess	Latitude	Longitude	Sample Collection Elevation (km)	Mean Drainage Elevation (km)	Sample Date
WS-1	Lake	9.34	15.52	-59.24	24.11	-104.55	1.863	1.86	10/26/19
WS-2	River	-9.09	-67.89	4.84	24.33	-103.43	1.928	1.93	10/26/19
WS-4	River	-9.59	-69.95	6.79	24.06	-104.53		1.87	10/26/19
WS-5	Rio Tunal River	-10.34	-74.38	8.32	24.03	-104.60	1.863	1.87	10/26/19
WS-6	Lake	6.44	11.40	-40.13	23.99	-104.77	1.983	2.19	11/1/19
WS-8	Spring	-8.37	-52.36	14.59	22.15	-104.79	1.988	1.62	10/29/19
WS-10	Lake	-3.11	-27.96	-3.11	23.94	-104.89	1.868	2.33	11/1/19
WS-14	Lake	-1.79	-25.69	-11.36	23.89	-105.06	2.079	2.55	11/1/19
WS-16	Lake	-12.71	-97.22	4.43	23.93	-103.17	1.868	2.01	10/26/19
WS-17	Lake	-5.19	-37.33	4.18	21.87	-105.15	1.593	0.08	10/29/19
WS-19	Lake	-10.82	-77.54	9.01	22.68	-103.74	0.082	2.23	10/27/19
WS-20	River	-7.83	-51.15	11.47	21.91	-105.18	1.047	0.02	10/29/19
WS-21	Lake	-4.28	-40.82	-6.61	23.46	-102.97	1.826	2.01	10/26/19
WS-22	River	-9.21	-67.43	6.24	23.18	-102.96	1.254	2.17	10/27/19
WS-24	Lake	-7.40	-54.67	4.52	23.11	-103.08	2.235	2.17	10/27/19
WS-25	River	-7.55	-56.38	4.00	22.72	-103.59	0.744	1.86	10/27/19
WS-26	Lake	-6.16	-55.03	-5.74	23.04	-103.16	0.475	2.15	10/27/19
WS-27	Lake	-7.24	-56.98	0.97	23.02	-103.20	1.66	2.17	10/27/19
WS-28	Lake	-5.40	-49.42	-6.20	22.85	-103.38	1.302	2.07	10/27/19
WS-29	Rio Valparaiso River	-9.08	-65.37	7.23	22.89	-103.36	1.64	2.12	10/27/19
WS-30	Lake	-3.40	-30.58	-3.35	23.87	-105.22	0.973	2.40	11/1/19
WS-32	Rio Valparaiso River	-9.10	-67.15	5.63	22.69	-103.60	0.295	1.84	10/27/19
WS-35	Spring	-8.21	-53.01	12.67	23.54	-105.84	0.295	2.06	11/1/19
WS-38	Rio San Pedro River	-7.67	-47.46	13.91	21.95	-105.22	2.037	0.00	10/30/19
WS-39	River	-6.11	-34.88	14.00	22.25	-105.31	0.013	0.07	10/30/19
WS-43	Lake	-2.87	-31.65	-8.69	23.83	-105.33	0.043	2.50	11/1/19
WS-45	Spring	-7.64	-46.87	14.21	23.46	-105.84	2.498	1.47	11/1/19
WS-46	Aguanavel River	-6.05	-50.98	-2.57	23.85	-103.02	2.743	1.86	10/26/19

<b>WS-47</b>	Lake	-3.59	-33.49	-4.74	22.81	-103.50	2.555	2.02	10/27/19
<b>WS-49</b>	River	-6.02	-39.56	8.58	23.01	-105.91	2.012	0.04	10/30/19
<b>WS-50</b>	Spring	-6.43	-38.74	12.70	23.40	-105.93	0.044	0.66	10/31/19
<b>WS-51</b>	Lake	-0.92	-15.23	-7.89	24.21	-103.34	1.896	2.12	10/26/19
<b>WS-53</b>	Lake	3.84	11.43	-19.28	23.29	-106.37	2.143	0.09	10/30/19
<b>WS-55</b>	Spring	-9.24	-60.27	13.68	23.76	-105.44	0.045	2.70	11/1/19
<b>WS-56</b>	River	-9.61	-60.45	16.47	23.66	-105.74	0.735	2.62	11/1/19
<b>WS-57</b>	River	-7.98	-52.47	11.40	23.76	-105.45	0.489	2.66	11/1/19
<b>WS-59</b>	Rio Valparaiso River	-8.68	-62.50	6.97	22.78	-103.55	0.452	1.89	10/27/19
<b>WS-63</b>	Spring	-5.83	-33.44	13.18	23.41	-105.90	0.405	0.83	10/31/19
<b>WS-64</b>	River	-11.87	-81.89	13.10	22.64	-104.12	0.436	1.25	10/27/19
<b>WS-66</b>	River	-9.09	-58.06	14.65	23.73	-105.57	0.286	2.78	11/1/19
<b>WS-68</b>	Lake	-7.97	-47.69	16.05	23.67	-105.72	0.304	2.71	11/1/19
<b>WS-69</b>	Lake	-5.69	-44.16	1.33	23.66	-105.78	0.407	2.35	11/1/19
<b>WS-70</b>	Spring	-8.89	-54.74	16.35	23.64	-105.83	0.319	2.43	11/1/19
<b>WS-71</b>	River	-6.51	-37.93	14.17	23.42	-105.86	2.055	1.26	11/1/19
<b>WS-72</b>	River	-10.56	-72.44	12.01	22.65	-104.14	0.325	1.30	10/27/19
<b>WS-73</b>	Lake	-3.59	-45.67	-16.92	22.62	-104.17	0.286	1.76	10/27/19
<b>WS-75</b>	Lake	-4.35	-33.16	1.64	23.57	-105.83	0.467	2.05	11/1/19
<b>WS-76</b>	River	-5.42	-32.41	10.98	23.32	-105.99	0.604	0.21	10/31/19
<b>WS-77</b>	River	-5.24	-29.49	12.41	23.35	-106.10	0.624	0.09	10/31/19
<b>WS-78</b>	Lake	0.17	-6.02	-7.40	23.35	-106.11	0.456	0.10	10/31/19
<b>WS-81</b>	Lake	-2.27	-17.83	0.33	23.32	-106.07	0.044	0.11	10/31/19
<b>WS-82</b>	Lake	-6.84	-54.69	0.03	22.54	-104.32	0.109	2.60	10/28/19
<b>WS-83</b>	River	-10.62	-70.25	14.71	22.62	-104.21	0.426	2.35	10/28/19
<b>WS-84</b>	Lake	-9.86	-81.47	-2.56	22.62	-104.19	0.308	2.07	10/27/19
<b>WS-85</b>	Lake	-10.35	-79.70	3.07	22.62	-104.25	0.385	2.65	10/28/19
<b>WS-86</b>	Lake	-10.58	-74.54	10.11	22.62	-104.26	2.166	2.65	10/28/19
<b>WS-87</b>	Lake	-8.41	-65.15	2.13	22.61	-104.27	2.164	2.66	10/28/19
<b>WS-88</b>	Lake	-13.21	-94.87	10.84	22.60	-104.29	1.898	2.75	10/28/19
<b>WS-89</b>	Lake	0.08	-21.84	-22.49	24.20	-104.48	2.219	1.86	10/26/19
<b>WS-90</b>	Lake	-6.45	-49.56	2.08	22.46	-104.30	2.161	2.44	10/28/19
<b>WS-91</b>	Lake	6.37	9.09	-41.88	24.21	-104.47	2.065	1.86	10/26/19
<b>WS-92</b>	Lake	-4.54	-38.83	-2.47	22.24	-104.58	2.067	0.78	10/29/19

<b>WS-93</b>	Lake	1.59	-16.81	-29.51	24.25	-104.44	2.076	1.87	10/26/19
<b>WS-94</b>	Lake	-6.29	-46.95	3.41	24.34	-104.31	2.134	2.03	10/26/19
<b>WS-95</b>	River	-7.87	-48.92	14.01	22.07	-104.81	1.899	1.00	10/29/19
<b>WS-96</b>	River	-7.44	-45.31	14.23	22.04	-104.82	0.248	0.36	10/29/19
<b>WS-97</b>	River	-6.52	-37.59	14.60	22.03	-104.94	0.044	0.19	10/28/19
<b>WS-98</b>	River	-6.35	-35.25	15.53	22.00	-104.95	0.474	0.21	10/29/19
<b>WS-99</b>	Tap	-5.47	-34.46	9.27	23.27	-106.38	1.862	0.03	10/30/19
<b>WS-103</b>	River	-9.17	-66.05	7.33	24.02	-104.56	2.502	1.87	10/26/19
<b>WS-104</b>	River	-8.28	-61.12	5.09	24.39	-104.27		1.99	10/26/19
<b>WS-105</b>	River	-9.64	-72.42	4.71	24.44	-104.11		1.99	10/26/19
<b>WS-106</b>	Lake	-4.23	-43.86	-10.04	24.28	-103.81	1.868	2.18	10/26/19
<b>WS-107</b>	Lake	-8.49	-66.73	1.16	24.23	-103.56	1.126	2.08	10/26/19
<b>WS-108</b>	Lake	-8.66	-65.59	3.71	24.29	-103.45	1.853	1.97	10/26/19
<b>WS-111</b>	Lake	-8.74	-69.61	0.33	22.65	-103.96	1.882	1.60	10/27/19
<b>WS-112</b>	River	-8.58	-68.74	-0.07	22.68	-103.98	0.244	1.33	10/27/19
<b>WS-113</b>	Lake	-9.62	-75.88	1.09	22.67	-104.09	1.869	1.10	10/27/19
<b>WS-114</b>	Spring	-8.25	-53.98	11.98	22.36	-104.35		1.83	10/28/19
<b>WS-115</b>	River	-7.84	-50.92	11.80	22.33	-104.39		1.25	10/28/19
<b>WS-116</b>	Lake	-9.25	-64.83	9.16	22.41	-104.35	0.257	2.38	10/29/19
<b>WS-117</b>	Lake	-7.94	-60.72	2.81	22.31	-104.44	2.039	0.75	10/29/19
<b>WS-118</b>	River	-7.82	-52.64	9.88	22.26	-104.50	0.123	0.48	10/29/19
<b>WS-119</b>	Spring	-8.89	-59.16	11.98	22.24	-104.61	2.799	1.30	10/29/19
<b>WS-120</b>	Lake	-7.08	-49.83	6.78	22.19	-104.68	1.976	1.30	10/29/19
<b>WS-121</b>	Spring	-9.14	-61.20	11.95	22.17	-104.75	2.632	1.46	10/29/19
<b>WS-122</b>	Spring	-6.78	-40.36	13.84	22.08	-104.81	1.88	1.01	10/29/19
<b>WS-123</b>	Lake	-7.17	-43.60	13.77	22.04	-104.87	2.043	0.24	10/29/19
<b>WS-124</b>	Lake	-6.33	-37.45	13.19	22.03	-104.89	0.251	0.19	10/29/19
<b>WS-127</b>	River	-5.92	-32.62	14.73	21.94	-105.02	1.281	0.06	10/29/19
<b>WS-129</b>	Rio San Pedro River	-5.79	-44.32	2.01	21.95	-105.22	2.673	0.02	10/30/19
<b>WS-130</b>	Pacific Ocean	-0.37	-1.02	1.98	21.99	-105.64	1.918	0.00	10/30/19
<b>WS-131</b>	Lake	-1.97	-17.85	-2.06	23.31	-106.32	1.927	0.06	10/30/19
<b>WS-132</b>	Lake	-8.58	-53.46	15.21	23.70	-105.72	0.027	2.74	11/1/19
<b>WS-201</b>	Spring	-8.4768	-51.8007	16.0138	24.75	-99.79		0.73	11/2/19
<b>WS-202</b>	Ojo de Agua Spring	-7.5304	-44.5527	15.6902	24.79	-99.70		0.49	11/2/19

<b>WS-203</b>	Lake	-6.1981	-37.2515	12.3335	24.79	-99.66	0.249	0.45	11/2/19
<b>WS-204</b>	Lake	-0.4817	-14.8572	- 11.0039	24.82	-99.60		0.41	11/2/19
<b>WS-205</b>	Lake	-6.1715	-34.7074	14.6643	24.79	-99.64	1.305	0.43	11/2/19
<b>WS-206</b>	Lake	-5.1501	-36.8727	4.3280	24.74	-99.41	1.756	0.29	11/3/19
<b>WS-207</b>	Lake	-5.5744	-30.1432	14.4517	24.66	-99.34	2.063	0.30	11/3/19
<b>WS-208</b>	River	-5.4475	-32.5387	11.0409	24.59	-99.18	0.229	0.41	11/3/19
<b>WS-209</b>	Spring	-4.9587	-31.0161	8.6536	24.52	-99.18	0.121	0.32	11/3/19
<b>WS-210</b>	Spring	-5.0914	-31.5704	9.1605	24.48	-99.14	0.118	0.32	11/3/19
<b>WS-211</b>	Lake	5.2409	19.8948	- 22.0322	24.44	-99.10	0.257	0.29	11/3/19
<b>WS-213</b>	River	-5.4083	-30.3593	12.9071	24.59	-98.95	1.64	0.47	11/3/19
<b>WS-214</b>	Lake	-5.7603	-37.8822	8.2006	24.72	-98.87	0.255	0.61	11/3/19

## References

- Adams, D. K., and Comrie, A. C. 1997. The North American monsoon. *Bulletin of the American Meteorological Society*, 78, 2197–2213.
- Baez-Gonzalez, A. D., Torres-Meza, M. D. J., Royo-Marquez, M. H. and Kiniry, J. R., 2018. Climate variability and trends in climate extremes in the priority conservation area El Tokio and adjacent areas in northeastern Mexico. *Weather and Climate Extremes*, 22, 36–47. doi: 10.1016/j.wace.2018.10.001.
- Bagheri, R., Bagheri, F., Karami, G. H. and Jafari, H., 2019. Chemo-isotopes ( $^{18}\text{O}$  and  $^2\text{H}$ ) signatures and HYSPLIT model application: Clues to the atmospheric moisture and air mass origins. *Atmospheric Environment*, 215, 116892. doi:10.1016/j.atmosenv.2019.116892.
- Barlow, M., Nigam, S. and Berbery, E. H. 1998. Evolution of the North American monsoon system. *Journal of Climate*, 11, 2238–2257.
- Bershaw, J. and Lechler, A. R. 2019. The isotopic composition of meteoric water along altitudinal transects in the Tian Shan of Central Asia. *Chemical Geology*, 516, 68–78.
- Bershaw, J. Penny, and S.M. Garzione, C.N. 2012. Stable isotopes of modern water across the Himalaya and eastern Tibetan Plateau: implications for estimates of paleoelevation and paleoclimate. *Journal of Geophysical Research: Atmospheres*, 117, 1–18. <https://doi.org/10.1029/2011JD016132>.
- Bershaw, J. Saylor, J. E., Garzione, C. N., Leier, A., and Sundell, K. E., 2016. Stable isotope variations ( $\delta^{18}\text{O}$  and  $\delta\text{D}$ ) in modern waters across the Andean Plateau. *Geochimica Et Cosmochimica Acta*, 194, 310–324. doi: 10.1016/j.gca.2016.08.011.
- Bryson, R. A. and Lowry, W. P. 1955. Synoptic climatology of the Arizona summer precipitation singularity. *Bulletin of the American Meteorological Society*, 36, 329–339.
- Cook, B. I. and Seager, R. 2013. The response of the North American Monsoon to increased greenhouse gas forcing. *Journal of Geophysical Research: Atmospheres*, 118, 1690–1699.

- Craig, H. 1961. Isotopic variations in meteoric waters. *Science* 133,1702–8.
- Curio, J., Maussion, F. and Scherer, D., 2015. A 12-year high-resolution climatology of atmospheric water transport over the Tibetan Plateau. *Earth System Dynamics*, 6(1), 109–124. doi: 10.5194/esd-6-109-2015.
- Dansgaard, W. 1953. The Abundance of O<sup>18</sup> in Atmospheric Water and Water Vapour. *Tellus*, 5(4). <https://doi.org/10.1111/j.2153-3490.1953.tb01076.x>.
- Dansgaard, W. 1964. Stable isotopes in precipitation. *Tellus*, 16, 436–68.
- Draxler, R.R. and Rolph, G.D. 2014. HYSPLIT (Hybrid Single-Particle Lagrangian Integrated Trajectory). *NOAA Air Resources Laboratory*, College Park, MD. Model access via NOAA ARL READY Website (<http://www.arl.noaa.gov/HYSPLIT.php>).
- Dutton, A., Wilkinson, B.H., Welker, J.M., Bowen, G.J. and Lohmann, K.C. 2005. Spatial distribution and seasonal variation in 18 O/16 O of modern precipitation and river water across the conterminous USA. *Hydrological Processes*, 19, 4121–4146. <https://doi.org/10.1002/hyp.5876>.
- Duprez, D. 2006. Study of surface reaction mechanisms by 16O/18O and H/D isotopic exchange. *Catalysis Today*, 112(1-4), 17–22. doi: 10.1016/j.cattod.2005.11.036.
- Fan, M., Heller, P., Allen, S. D. and Hough, B. G. 2014. Middle Cenozoic uplift and concomitant drying in the central Rocky Mountains and adjacent Great Plains. *Geology*, 42(6), 547-550.
- Fan, M., Hough, B.G. and Passey, B.H. 2014b. Middle to late Cenozoic cooling and high topography in the central Rocky Mountains: constraints from clumped isotope geochemistry. *Earth and Planetary Science Letters*, 408, 35–47. <https://doi.org/10.1016/j.epsl.2014.09.050>.
- Fawcett, P. J., Stalker, J. R. and Gutzler, D. S. 2002. Multistage moisture transport into the interior of northern Mexico during the North

- American summer monsoon. *Geophysical Research Letters*, 29(23). doi: 10.1029/2002gl015693.
- Garziona C.N., Quade J., DeCelles P.G. and English NB. 2000b. Predicting paleoelevation of Tibet and the Himalaya from  $d^{18}O$  vs altitude gradients in meteoric water across the Nepal Himalaya. *Earth and Planetary Science Letters*, 183, 215–29.
- Gat, J. R. 1996. Oxygen And Hydrogen Isotopes In The Hydrologic Cycle. *Annual Review of Earth and Planetary Sciences*, 24(1), 225–262. doi: 10.1146/annurev.earth.24.1.225
- Gat, J.R. and Airey, P.L. 2006. Stable water isotopes in the atmosphere/biosphere/lithosphere interface: scaling-up from the local to continental scale, under humid and dry conditions. *Global and Planetary Change*, 51, 25–33. <https://doi.org/10.1016/j.gloplacha.2005.12.004>.
- Gat, J.R. and Dansgaard, W. 1972. Stable isotope survey of the freshwater occurrences in Israel and the Northern Jordan Rift Valley. *Journal of Hydrology*, 16, 177–211. [https://doi.org/10.1016/0022-1694\(72\)90052-2](https://doi.org/10.1016/0022-1694(72)90052-2).
- Gat, J.R. and Lister GS. 1995. The “catchment effect” on the isotopic composition of lake waters; its importance in paleolimnological interpretations. In *Proceedings European Science Foundation Workshop*, In press.
- Hoefs, J., 2018. Stable Isotope Geochemistry. *Springer International Publishing*. 10.1007/978-3-319-78527-1.
- International Atomic Energy Agency. 2019. *Water Isotope System For Data Analysis Visualization And Electronic Retrieval*.
- IAEA/WMO (2019). Global Network of Isotopes in Precipitation. The GNIP Database. Accessible at: <https://nucleus.iaea.org/wiser>.
- Jackson, L. J., Horton, B. K., Beate, B. O., Bright, J. and Breecker, D. O. 2019. Testing stable isotope paleoaltimetry with Quaternary

- volcanic glasses from the Ecuadorian Andes. *Geology*, 47(5), 411–414. doi: <https://doi.org/10.1130/G45861.1>
- Kendall, C. and Coplen, T.B. 2001. Distribution of oxygen-18 and deuterium in river waters across the United States. *Hydrological Processes*, 15, 1363–1393. <https://doi.org/10.1002/hyp.217>.
- Kumar, A., Tiwari, S., Verma, A. and Gupta, A. 2018. Tracing isotopic signatures ( $\delta D$  and  $\delta^{18}O$ ) in precipitation and glacier melt over Chorabari Glacier–Hydroclimatic inferences for the Upper Ganga Basin (UGB), Garhwal Himalaya . *Journal of Hydrology: Regional Studies*, 15, 68-89.
- Lehmann, M. and Siegenthaler, U. 1991. Equilibrium oxygen- and hydrogen-isotope fractionation between ice and water. *Journal of Glaciology*, 37(125), 23–26. doi: 10.3189/s0022143000042751.
- Li, L. and Garzione, C.N. 2017. Spatial distribution and controlling factors of stable isotopes in meteoric waters on the Tibetan Plateau: implications for paleoelevation reconstruction. *Earth and Planetary Science Letters*, 460, 302–314. <https://doi.org/10.1016/j.epsl.2016.11.046>.
- Licht, A., Quade, J., Kowler, A., De Los Santos, M., Hudson, A., Schauer, A., Huntington, K., Copeland, P. and Lawton, T. 2017. Impact of the North American monsoon on isotope paleoaltimeters: implications for the paleoaltimetry of the American southwest. *American Journal of Science*, 317, 1–33. <https://doi.org/10.2475/01.2017.01>.
- McDowell, F. 2007. Geologic Transect Across the Northern Sierra Madre Occidental Volcanic Field, Chihuahua and Sonora, Mexico. *Geological Society of America*.
- Morrone, J. J., Organista, D. E. and Bousquets, J. L. 2002. Mexican biogeographic provinces: preliminary scheme, general characterizations, and synonymies. *Acta Zoologica Mexicana*, 85. doi: 10.11646/zootaxa.4277.2.8
- NARR, 2019. NARR data provided by the NOAA/OAR/ESRL PSD, Boulder, Colorado, USA, from their Web site at <http://www.esrl.noaa.gov/psd/>.

- Poage, M.A. and Chamberlain, C.P. 2001. Empirical relationships between elevation and the stable isotope composition of precipitation and surface waters: considerations for studies of paleoelevation change. *American Journal of Science*, 301,1–15.
- Rowley, D. B. and Garzione, C. N. 2007. Stable Isotope-Based Paleoaltimetry. *Annual Review of Earth and Planetary Sciences*, 35(1), 463–508. doi: 10.1146/annurev.earth.35.031306.140155.
- Schmitz, J. T. and Mullen, S. L. 1996. Water Vapor Transport Associated with the Summertime North American Monsoon as Depicted by ECMWF Analyses. *Journal of Climate*, 9(7), 1621–1634. doi: 10.1175/1520-0442(1996)009<1621:wvtawt>2.0.co;2.
- Sharp, Z., 2007. *Principles of Stable Isotope Geochemistry* (2nd ed.). Upper Saddle River, NJ: Pearson/Prentice Hall.
- Stensrud, D. J., Gall, R. L., Mullen, S. L. and Howard, K. W. 1995. Model Climatology of the Mexican Monsoon. *Journal of Climate*, 8(7), 1775–1794. doi: 10.1175/1520-0442(1995)008<1775:mcotmm>2.0.co;2.
- Wassenaar, L., Wilgenburg, S. V., Larson, K. and Hobson, K. 2009. A groundwater isoscape ( $\delta D$ ,  $\delta^{18}O$ ) for Mexico. *Journal of Geochemical Exploration*, 102(3), 123–136. doi: 10.1016/j.gexplo.2009.01.001.
- Zhu, L., Fan, M., Hough, B. and Li, L. 2018. Spatiotemporal distribution of river water stable isotope compositions and variability of lapse rate in the central Rocky Mountains: Controlling factors and implications for paleoelevation reconstruction. *Earth and Planetary Science Letters*, 496, 215-226.

## Biographical Information

Jordan received her bachelor's degree in Professional Geology at the University of Wisconsin – Oshkosh and her master's degree in Petroleum Geology from the University of Texas at Arlington, as well as her Master of Legal Studies in Oil, Gas and Energy Law from the University of Oklahoma. She has worked on research projects including stable isotope chemistry, hydrology, metamorphic petrology, glacial mapping and trace element analysis. Her interests include petroleum exploration, such as geologic mapping, geophysics and seismic interpretation and land management. She plans to pursue a career in the petroleum exploration sector.